

MicroRNA134 of Ventral Hippocampus Is Involved in Cocaine Extinction-Induced Anxiety-like and Depression-like Behaviors in Mice

Yuehan Li,^{1,2,5} Xue Lu,^{1,5} Jiaxun Nie,¹ Panpan Hu,³ Feifei Ge,^{1,2} Ti-Fei Yuan,⁴ and Xiaowei Guan^{1,2}

¹Department of Human Anatomy and Histoembryology, Nanjing University of Chinese Medicine, Nanjing, China; ²Jiangsu Key Laboratory for Pharmacology and Safety Evaluation of Chinese Materia Medica, Nanjing University of Chinese Medicine, Nanjing, China; ³Department of Human Anatomy, Nanjing Medical University, Nanjing, China; ⁴Shanghai Key Laboratory of Psychotic Disorders, Shanghai Mental Health Center, Shanghai Jiaotong University, Shanghai, China

We previously found that cocaine abuse could increase microRNA134 (miR134) levels in the hippocampus; yet the roles of miR134 in cocaine-related abnormal psychiatric outcomes remain unknown. In this study, using the cocaine-induced conditioned place preference (CPP) mice model, we found that mice exhibit enhanced anxiety-like and depression-like behaviors during the cocaine extinction (CE) period of CPP, accompanied by obviously increased miR134 levels and decreased levels of 19 genes that are associated with synaptic plasticity, glia activity, and neurochemical microenvironments, in the ventral hippocampus (vHP). Knockdown of miR134 in vHP *in vivo* reversed the changes in 15 of 19 potential gene targets of miR134 and rescued the abnormal anxiety-like and depression-like behavioral outcomes in CE mice. In parallel, knockdown of miR134 reversed CE-induced changes in dendritic spines and synaptic proteins and increased the field excitatory postsynaptic potential (fEPSP) of CA1 pyramidal neurons in the vHP of CE mice. In addition, knockdown of miR134 suppressed the CE-enhanced microglia activity, inflammatory, apoptotic, and oxidative stress statuses in the vHP. With the data taken together, miR134 may be involved in cocaine-associated psychiatric problems, potentially via regulating the expressions of its gene targets that are related to synaptic plasticity and neurochemical microenvironments.

INTRODUCTION

Cocaine addiction is characterized by a loss of control over drug intake and a high rate of relapse.^{1,2} In both humans³ and rodents,^{4,5} psychostimulants could enhance anxiety and depression behaviors, which contribute to relapse to the drugs.^{2,6} In recent decades, microRNAs (miRNAs) have been extensively studied in the abuse of psychostimulants such as cocaine.^{7–9} Previously, we found a remarkable increase of miRNA 134 (miR134) in rat hippocampus during the extinction period of cocaine-induced conditioned place preference (CPP),¹⁰ yet whether and how miR134 is involved in cocaine-related abnormal behaviors remain unknown.

miRNAs are small, endogenous, non-protein-coding RNA molecules that regulate gene expression by interacting with target genes.¹¹ In particular, miRNAs have emerged as promising diagnostic markers

and novel therapeutic targets against anxiety,¹² depression,¹³ and cocaine addiction.¹⁴ miR134 is enriched in the hippocampus.^{9,15} miR134 plays important roles in the regulation of the size⁹ and volume¹⁶ of dendritic spines^{17,18} and might be implicated in glia activity and neurochemical microenvironments around neurons. The hippocampus is one of the brain regions that are most sensitive to the psychostimulants' neurotoxicity and plays a major role in cocaine addiction.^{19,20} The ventral hippocampus (vHP) has prominent roles in emotional processes such as anxiety, depression, fear, and stress.^{21,22}

In the present study (Figure 1A), we propose a link between abnormal behaviors and the miR134 in cocaine-exposed mice. miR134 of vHP might be involved in cocaine-induced abnormal behavioral outcomes through regulating its target genes and subsequent synaptic plasticity as well as neurochemical microenvironments in the vHP. Managing the miR134 signal pathway in the vHP might be an effective approach for the treatment of abnormal behaviors caused by cocaine use.

RESULTS

miR134-5P Levels Were Increased in the vHP during the Cocaine Extinction (CE) Period, and Knockdown of miR134 in vHP Rescued the Enhanced Anxiety-like and Depression-like Behaviors in CE Mice

To assess CE models, the CPP procedure was used in mice (Figure 1B). Saline-extinction (SE)-treated mice were used as controls.

Received 30 June 2019; accepted 24 December 2019;
<https://doi.org/10.1016/j.omtn.2019.12.030>

⁵These authors contributed equally to this work.

Correspondence: Feifei Ge, Department of Human Anatomy and Histoembryology, Nanjing University of Chinese Medicine, 138 Xianlin Ave., Nanjing 210023, China.

E-mail: fge@njucm.edu.cn

Correspondence: Ti-Fei Yuan, Shanghai Key Laboratory of Psychotic Disorders, Shanghai Mental Health Center, Shanghai Jiaotong University, 600 Wanping Road, Shanghai 200030, China.

E-mail: ytf0707@126.com

Correspondence: Xiaowei Guan, Department of Human Anatomy and Histoembryology, Nanjing University of Chinese Medicine, 138 Xianlin Ave., Nanjing 210023, China.

E-mail: guanxw918@njucm.edu.cn



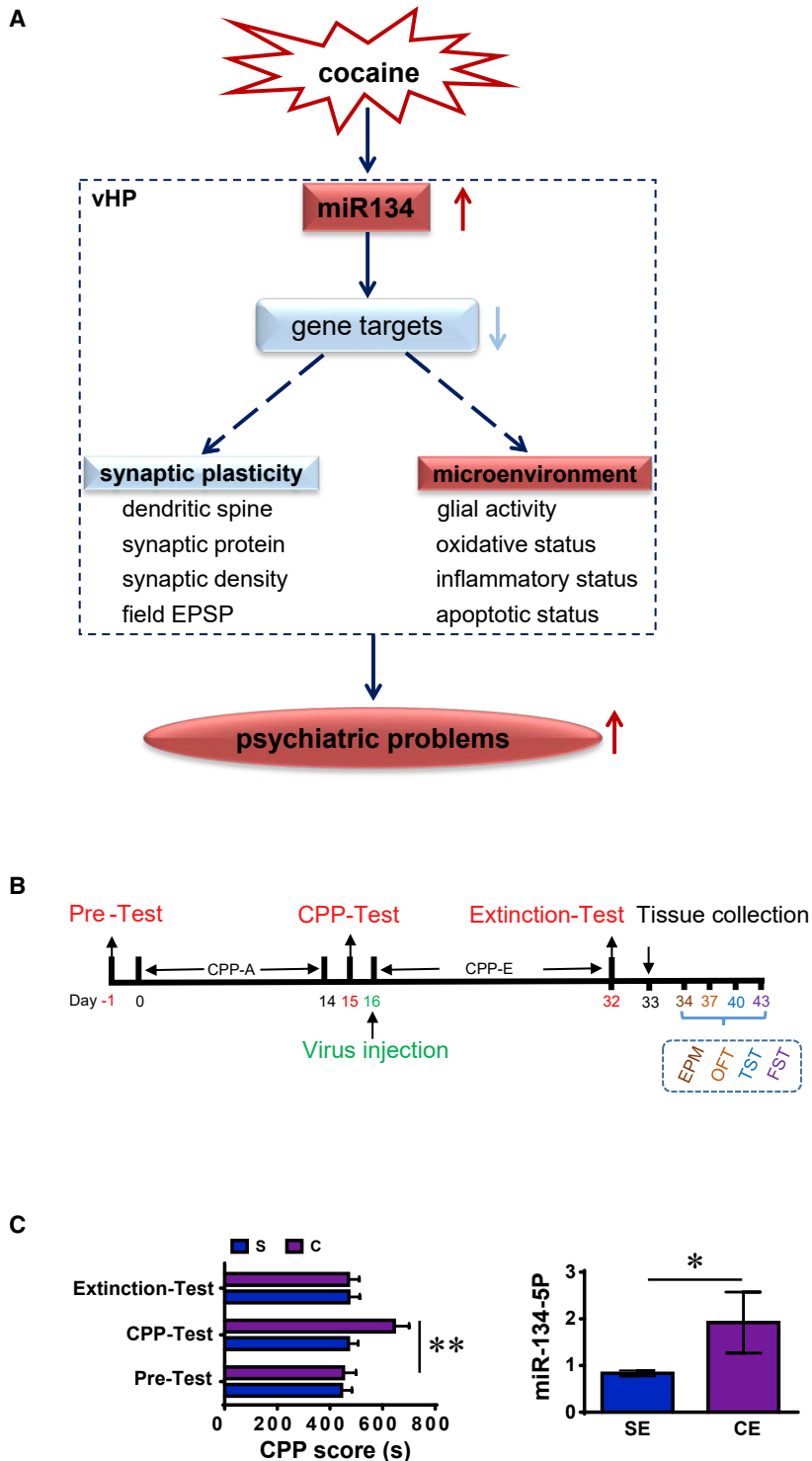


Figure 1. miR134-5P Level Is Increased by CE in the vHP of Mice

(A) Proposed model of the present study. (B) Experimental design and timeline. (C) CPP scores (left, $n = 16$) and miR134-5P levels (right, $n = 6$) of vHP. CPP, conditioned place preference; CE, cocaine extinction mice; EPM, elevated plus maze; OFT, open field test; TST, tail suspension test; FST, forced swim test; SE, saline extinction mice; vHP, ventral hippocampus. ** $p < 0.01$, versus SE mice; N.S., $p > 0.05$, versus SE mice.

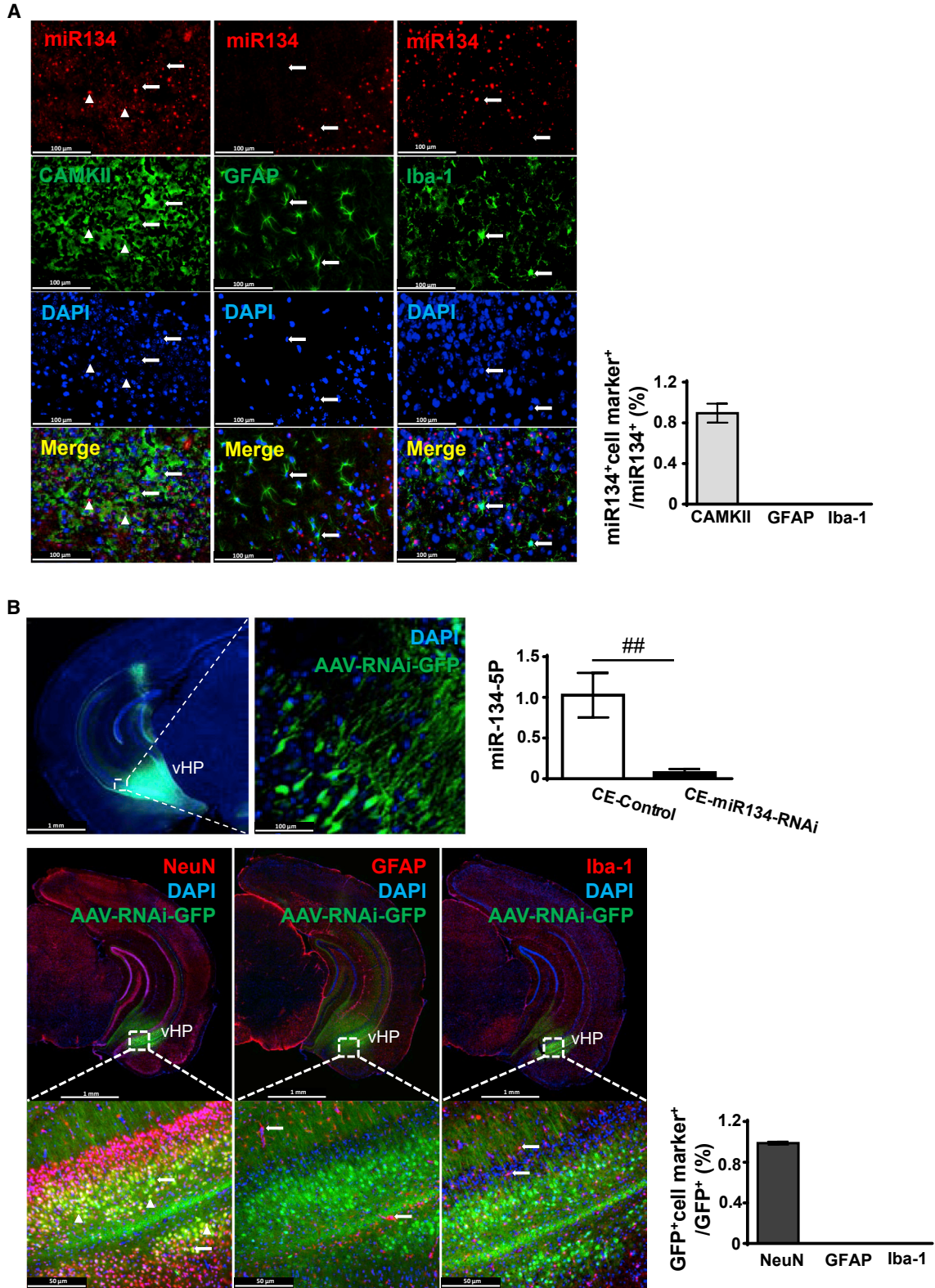
that cocaine CPP acquisition and extinction were successfully established in mice in the present study. By contrast, saline treatment could cause neither CPP acquisition nor extinction (SE) in mice. In parallel, miR134-5P levels were significantly increased in the vHP of CE mice when compared to that of SE mice after the extinction training ($t(4) = 2.9$, $p = 0.0458$; Figure 1C, right).

To assess the cell types in the vHP that miR134 is mainly expressed, the BaseScope method combined with immunostaining of specific cell markers was used in naive mice. As shown in Figure 2A, miR134 mostly colabeled with CAMKII, a marker of pyramidal neurons, but not with GFAP (glial fibrillary acidic protein, a marker of astrocyte) and Iba-1 (a marker of microglia) in the vHP, indicating that miR134 is mainly located in neurons of the vHP.

In this study, an adeno-associated virus (AAV), AAV9-mmu-miR134-5P-RNAi-GFP (miR134-RNAi-virus), was microinjected into the bilateral vHP of CE mice (CE-miR134-RNAi mice) to knock down miR134 expression *in vivo*. In order to evaluate miR134-RNAi-virus-transfected efficiency and transfected cell types in the vHP of CE mice, quantification of miR134-5P (compared with controlled virus-injected CE mice; CE-control mice) and the localization of GFP with specific cell markers were examined in the CE mice. As shown at the top of Figure 2B, the AAV was mainly injected into vHP and about 93% of miR134 was knocked down by miR134-RNAi-virus in the CE mice ($t(4) = 6$, $p = 0.004$ versus

CE-control). In addition, miR134-RNAi-virus was mostly transfected in neurons, as indicated by co-localization of GFP with NeuN (a marker of neuron), but not GFAP and Iba-1 (Figure 2B, middle and bottom).

As shown in the left panel of Figure 1C, mice spent more time in the cocaine-paired chamber after 14-day cocaine administration ($p < 0.01$, versus pre-test) and similar time after the subsequent 18-day extinction training ($p > 0.05$, versus pre-test), indicating



(legend on next page)

Knockdown of miR134 in the vHP Rescued the Enhanced Anxiety-like and Depression-like Behaviors in CE Mice

In this study, the elevated plus maze (EPM) and open field test (OFT) were used to assess anxiety-like behaviors, while the tail suspension test (TST) and forced swim test (FST) were used to examine depression-like behaviors in mice. CE mice spent less time in the open arms ($t(22) = 9.008$, $p < 0.0001$, versus SE mice; **Figure 3A**, left) of the EPM and in the central zone ($t(22) = 5.182$, $p < 0.0001$, versus SE mice; **Figure 3B**, middle) of the OFT, indicating the enhanced anxiety-like behaviors by CE exposure in mice. The distance traveled in the OFT apparatus did not differ between groups ($t(22) = 0.5555$, $p = 0.5841$; **Figure 3B**, left), indicating that CE did not influence the locomotive ability of mice. In both the TST ($t(22) = 6.870$, $p < 0.0001$; **Figure 3C**, left) and the FST ($t(22) = 8.938$, $p < 0.0001$; **Figure 3D**, left), the immobility times were higher in CE mice than in SE mice, indicating enhanced depression-like behaviors in CE mice. These enhanced anxiety-like and depression-like behaviors were rescued by knockdown of miR134 in the vHP, as indicated by decreased time spent in the open arms ($t(22) = 5.384$, $p < 0.0001$, versus CE-control; **Figure 3A**, right) of the EPM and the central zone ($t(22) = 5.091$, $p < 0.0001$, versus CE-control; **Figure 3B**, right) of the OFT for CE-miR134-RNAi mice, as well as decreased immobility time in the TST ($t(22) = 8.862$, $p < 0.0001$, versus CE-control; **Figure 3C**, right) and the FST ($t(22) = 5.999$, $p < 0.0001$, versus CE-control; **Figure 3D**, right) for the CE-miR134-RNAi mice.

Potential Gene Targets of miR134 that Involved in CE Were Scanned in the vHP of Mice

Based on the miRBase database (<http://www.mirbase.org/>) and references that were searched with the keywords “miRNA,” “plasticity,” and “glia,” 49 potential gene targets of miR134 were selected and quantified in the vHP. As shown in the left panel of **Figure 4A**, 19 of 49 genes decreased ($p < 0.05$, $p < 0.01$ versus SE) by CE, therefore being regarded as gene target candidates of miR134. After miR134-RNAi-virus treatment, 15 of the 19 gene target candidates were increased in the vHP of CE-miR134-RNAi mice ($p < 0.05$, $p < 0.01$ versus CE-control; **Figure 4A**, right), suggesting that these 15 genes may be involved in CE-related neuroadaptations as the downstream targets of miR134 in the vHP.

In order to further clarify the mRNA results of this study, the proteins coded by the several mRNAs of the 15 target genes of miR134 were quantified in the vHP. As shown in **Figure 4B**, all the tested proteins—including CREB, BDNF, SNAP23, STXBP5, and TICAM2—were decreased by CE in mice ($p < 0.05$, $p < 0.01$ versus SE) but

were reversed to higher levels by knocking down the miR134-5P in CE-miR134-RNAi mice ($p < 0.05$, $p < 0.01$ versus CE-control).

Knockdown of miR134 in the vHP Ameliorated the Changes in Synaptic Plasticity in CE Mice

The density of dendritic spine and synapse and the levels of synaptic proteins were examined to assess the synaptic plasticity in the vHP of mice. As shown in **Figure 5**, both the density of dendritic spines ($t(10) = 5.469$, $p = 0.0003$; **Figure 5A**, left) and density of synapses ($t(10) = 4.802$, $p = 0.0004$; **Figure 5B**) were significantly decreased, when compared with that of SE mice. In parallel, remarkable decreases of synapsin I (SYP I) ($t(4) = 3.183$, $p = 0.0334$) and PSD-95 ($t(4) = 2.944$, $p = 0.0422$) protein levels were observed in CE mice, when compared with that of SE mice (**Figure 5C**, left).

Knockdown of miR134 in the vHP reversed some changes in synaptic plasticity by CE, as indicated by an increased density of dendritic spines ($t(10) = 4.466$, $p = 0.0012$; **Figure 5A**, right) and protein levels of SYP I ($t(4) = 3.236$, $p = 0.0318$) and PSD-95 ($t(4) = 4.315$, $p = 0.0125$; **Figure 5C**, right) in the vHP of CE-miR134-RNAi mice when compared with that in CE-control mice. In parallel, knockdown of miR134 significantly enhanced the theta burst stimulation (TBS)-induced field excitatory postsynaptic potential (fEPSP) of CA1 pyramidal neurons in the vHP of CE mice ($p < 0.01$ versus CE-control; **Figure 5D**), indicating a negative regulation of miR134 in the development of long-term potentiation (LTP) of the vHP during CE.

Knockdown of miR134 Reversed the Changes in Microglia Activity and Neurochemical Microenvironments by CE in the vHP

In this study, GFAP and Iba-1 were used as marks for astrocyte and microglia, respectively, and the neurochemical microenvironments—including pro-inflammation factors, apoptotic molecules, and oxidative stress status—were examined in the vHP. As shown in the left panel of **Figure 6A**, the protein levels of Iba-1 ($t(4) = 6.7$, $p = 0.0428$), but not GFAP ($t(4) = 0.1891$, $p = 0.8592$), were significantly increased in the vHP of CE mice compared with that in SE mice. Levels of pro-inflammatory factors, including interleukin (IL)-6 ($t(4) = 2.895$, $p = 0.0444$), IL-1 β ($t(4) = 6.7$, $p = 0.0026$), tumor necrosis factor alpha (TNF- α) ($t(4) = 9.87$, $p = 0.0006$), and nuclear factor κ B (NF- κ B) ($t(4) = 2.888$, $p = 0.0447$), were increased by CE in the vHP (**Figure 6B**, left). Levels of apoptotic molecules such as caspase-3 (CAS3) ($t(4) = 3.265$, $p = 0.0309$), Bcl-2 ($t(4) = 4.427$, $p = 0.0114$), and Bcl-2 associated X protein (Bax) ($t(4) = 6.401$, $p = 0.0031$) were increased in the vHP of CE mice (**Figure 6C**, left).

Figure 2. miR134-Expressed and miR134-RNAi-virus-Transfected Cell Types in the vHP

(A) Illustration of miR134-expressed cell types in the vHP of native mice (left). White arrows indicate positive staining of biomarkers for cell types (green indicates CAMKII, GFAP, and Iba-1); white triangles indicate colocalization with miR134 (red) and biomarkers (green). Scale bars, 100 μ m. Ratio of colocalization with miR134 and biomarkers to miR-134-positive cells (right). (B) Illustration of miR134-RNAi-virus-transfected cell types in the vHP. Top panels: the injection site of virus (green, left; scale bar, 1 mm), expression of virus (green, middle; scale bar, 100 μ m), and miR-134-5P levels (right) in the vHP of CE mice. Middle panels: injection site of virus (green; scale bars, 1 mm). Bottom panels: miR134-RNAi-virus-transfected cell types in the vHP (left). White arrows indicate positive staining of biomarkers for cell types (red indicates NeuN, GFAP, and Iba-1); white triangles indicate colocalization with GFP (green) and biomarkers (red). Scale bars, 50 μ m. Ratio of colocalization with GFP and biomarkers to GFP-positive cells (right).

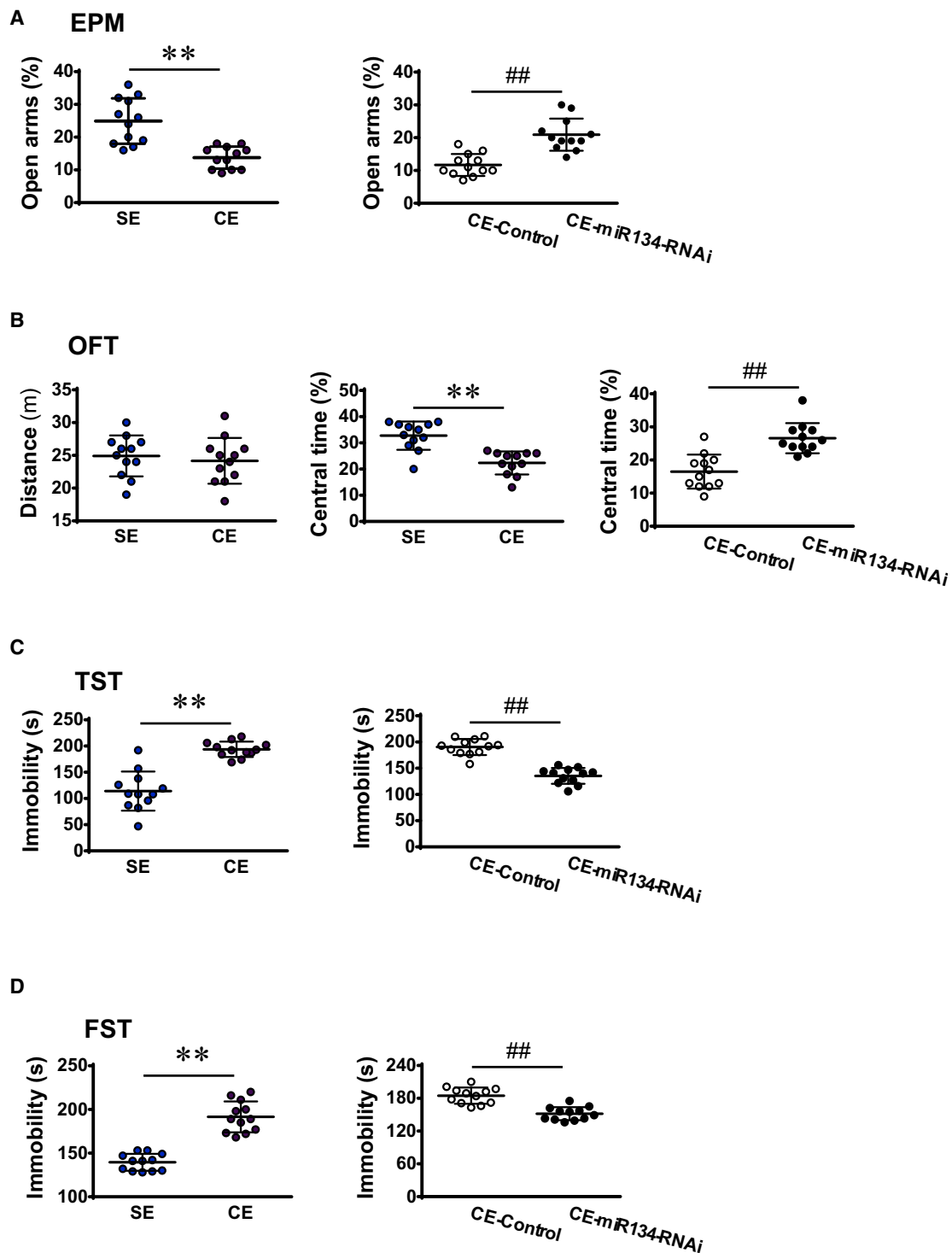


Figure 3. Knockdown of miR134 in the vHP Rescues CE-Enhanced Anxiety-like and Depression-like Behaviors in Mice

(A) EPM. Percentage of time spent in the open arms of EPM in SE and CE mice (left, n = 24), as well as in miR134 RNAi and controlled RNAi of CE mice (right, n = 24). (B) OFT. Distance traveled in the OFT apparatus (left); percentage of time spent in the central zone of the OFT (middle) in SE and CE mice (n = 24), as well as that in miR134 RNAi and

(legend continued on next page)

In parallel, activities of superoxide dismutase (SOD) ($t_{12} = 3.405$, $p = 0.0067$) were decreased, and levels of malondialdehyde (MDA) ($t_{12} = 3.802$, $p = 0.0034$) were increased in the vHP of CE mice compared with that of SE mice (Figure 6D, left).

Knockdown of miR134 reversed the higher statuses in microglial activity, inflammation, apoptosis, and oxidative stress by CE in the vHP, as indicated by the attenuated levels of Iba-1 ($t(4) = 6.505$, $p = 0.0029$; Figure 6A, right), IL-6 ($t(4) = 3.926$, $p = 0.0172$), IL-1 β ($t(4) = 5.366$, $p = 0.0058$), TNF- α ($t(4) = 6.777$, $p = 0.0025$), NF- κ B ($t(4) = 5.89$, $p < 0.0001$; Figure 6B, right), CAS3 ($t(4) = 6.278$, $p = 0.0033$), Bax ($t(4) = 3.206$, $p = 0.0327$; Figure 6C, right), and MDA ($t(12) = 4.974$, $p = 0.0006$; Figure 6D, right) and increased SOD ($t(12) = 8.399$, $p < 0.0001$) activity in the vHP of CE-miR134-RNAi mice, when compared with those in CE-control mice. In parallel, knockdown of miR134 failed to affect the levels of GFAP ($t(4) = 0.18$, $p = 0.8664$) and Bcl-2 ($t(4) = 5.135$, $p = 0.6188$) in the vHP of CE-experienced mice.

DISCUSSION

Cocaine addicts with high anxiety and depression levels are likely to relapse to drug use.^{2,6} In this study, CE exposure triggered an increase of miR134 level in the vHP, accompanied by changes in several potential target genes, synaptic plasticity, glia activity, and neurochemical microenvironments. Local knockdown of miR134 expression *in vivo* rescued the abnormal behaviors and reversed CE-induced changes in target genes, synaptic plasticity, glia activity, and microenvironment in the vHP of mice.

miR134 Is Involved in CE-Enhanced Anxiety-like and Depression-like Behaviors in Mice

miR134 is abundantly expressed in hippocampus. Several studies demonstrated that miR134 expressions are significantly increased^{17,23–25} or decreased^{7,26} in nervous diseases, such as seizure, ischemic stroke, and neuropathic pain. Blockade or activation of miR134 could suppress brain damage,^{15,27} suggesting that targeting miR134 signaling has potential therapeutic effects on brain disorders. Previously, we found a remarkable upregulation of the miR134 level in the intact hippocampus by cocaine exposure.¹⁰ Here, we further investigated the expression of miR134 in the ventral part of hippocampus, a brain region that is closely associated with the regulation of emotions such as anxiety, depression, stress, and fear. Consistent with previous results, CE significantly triggered miR134 expression in the vHP, accompanied by enhanced anxiety-like and depression-like behaviors in mice. A recent study reports that silencing miR134 in the brain alleviates depression-like behavior induced by chronic stress exposure in animals.²⁴ Similarly, we found that local knockdown of miR134 expression in the vHP reduced anxiety-like and depression-like behaviors in CE mice, sug-

gesting an involvement of miR134 in cocaine-use-related psychiatric problems.

Drug-induced neurotoxicity depends on changes in gene expression.²⁸ Based on a miRNA database (<http://www.mirbase.org/>) and previous reports of miR134 and nervous system diseases, we scanned 49 potential target genes of miR134 and found that 19 of them were decreased by CE in the vHP (Figure 4A). Importantly, knockdown of vHP miR134 *in vivo* could restore 15 gene levels of them, indicating that these 15 genes were regulated by miR134, which was involved in CE-induced abnormal behavioral outcomes. Further, we also examined the protein levels of CREB, BDNF, SNAP23, STXBP5, and TICAM2, which were consistent with the mRNA results. It has been well established that miRNAs act by binding to target mRNAs and initiating either cleavage or a reduction in the translational efficiency of the target mRNA, depending on the degree of sequence complementarity.²⁹ Based on the TargetScan database, miR134-5p and *Creb1* have predicted a consequential pairing of the target region. Studies also show that *Creb-1* and *Bdnf* are important molecular mechanisms underlying the plasticity deficit that are regulated by miR134.^{27,30,31} In the present study, we found that miR134 was predicted to target *Creb-1* and post-transcriptionally regulated the expression of CREB and BDNF in CE mice, which was consistent with previous results. In addition, we also identified other genes regulated by miR134. Some of them are closely involved in synaptic plasticity and transmission, such as *Snap23*, *Sypl2*, *Stxbp5*, *Stxbp1*, *Nfib*, *Grik3*, *Gnao1*, and *Drd5*;^{15,32,33} some contribute to glia and related microenvironments around neurons, such as *Bdnf*, *Snap23*, *Ticam2*, *Ndnf*, *Nanog*, and *Cdh9*; and most of them play important roles in psychiatric disorders, including depression, addiction, and epilepsy.^{34,35} Although no existing evidence has demonstrated that they have a direct complementary sequence of miR134, our results confirmed that these 15 genes were directly or indirectly regulated by miR134. We think that these target genes might be downstream of the miR134 directly regulated genes, such as *Bdnf* being regulated by *Creb1* expression.

miR134 Is Involved in CE-Caused Changes in Synaptic Plasticity in vHP of Mice

Until now, no effective therapeutic medicine has been available for the treatment of addiction, partially because addictive drugs of abuse lead to complicated changes in gene expression and subsequent plasticity in the brain. Schrott et al.⁹ first reveal that miR134 is expressed near synaptic sites on dendrites and enriched in synaptoneurosome. Later, Numakawa et al.³⁶ show a glial role of miR134 in relation to basic fibroblast growth factor (bFGF) function in astrocyte. It is intriguing to explore whether the altered levels of miR134 in vHP are a neuronal or glial response. In this study, BaseScope data showed that the expression of miR134 in the vHP was highly restricted in neurons,

controlled RNAi of CE mice (right, $n = 24$). (C) TST. Immobility time during the TST in SE and CE mice (left, $n = 24$), as well as in miR134 RNAi and controlled RNAi of CE mice (right, $n = 24$). (D) FST. Immobility time during the FST in SE and CE mice (left, $n = 24$), as well as in miR134 RNAi and controlled RNAi of CE mice (right, $n = 24$). ** $p < 0.01$ versus SE mice; ## $p < 0.01$ versus CE-control mice. CE, cocaine extinction mice; SE, saline extinction mice; CE-control, controlled RNAi-injected CE mice; CE-miR134-RNAi, miR134-RNAi-injected CE mice.

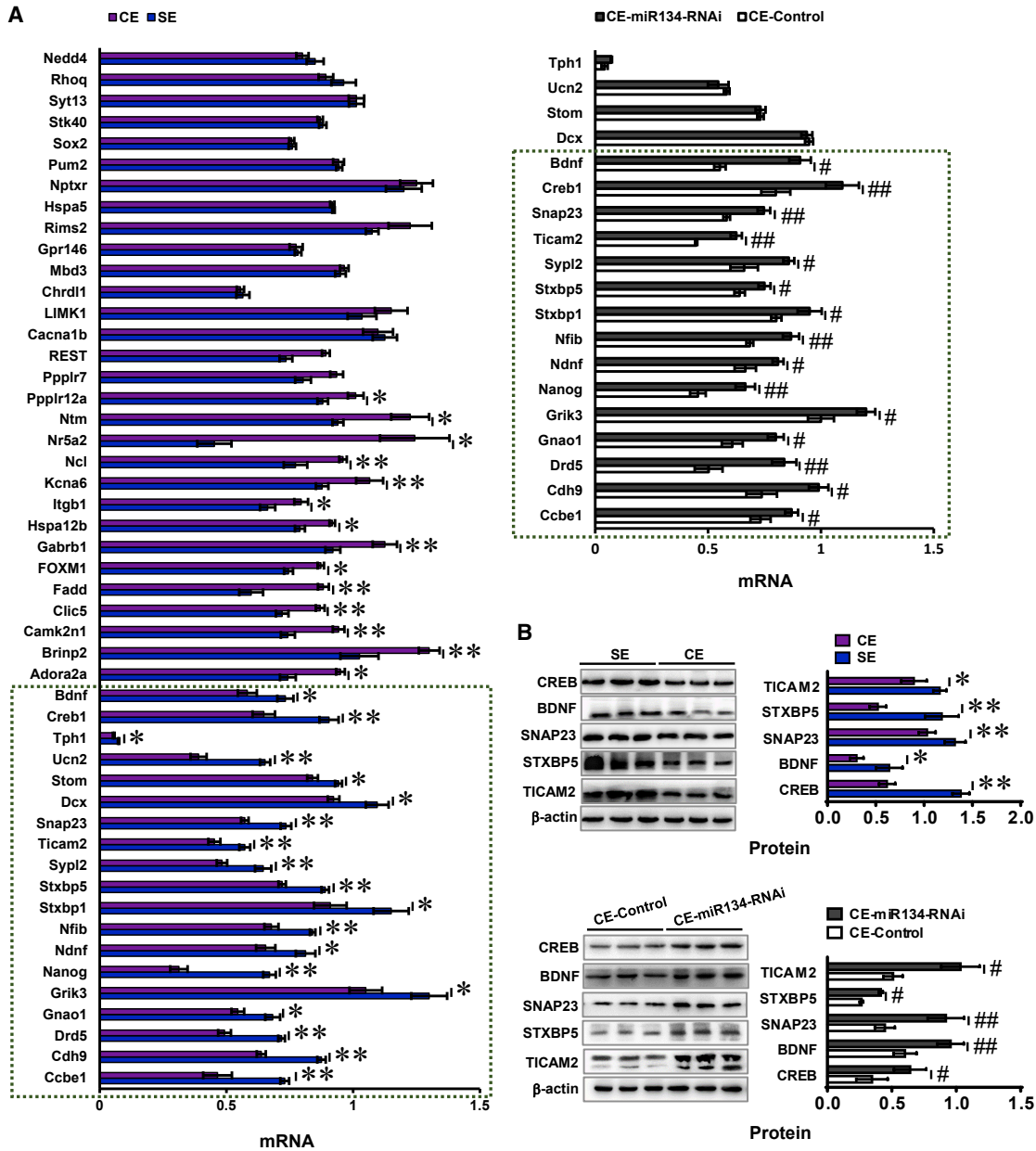


Figure 4. Target Gene Candidates of miR134 Are Scanned in Mice

(A) mRNA levels of potential miR134 target genes in SE and CE mice (left, $n = 12$), as well as in miR134 RNAi and controlled RNAi of CE mice (right, $n = 12$). (B) Protein levels of miR134 target gene candidates in SE and CE mice (top, $n = 6$), as well as in miR134 RNAi and controlled RNAi of CE mice (bottom, $n = 6$). * $p < 0.05$, and ** $p < 0.01$, versus SE mice; # $p < 0.05$, and ### $p < 0.01$, versus CE-control mice. CE, cocaine extinction mice; SE, saline extinction mice; CE-control, controlled RNAi-injected CE mice; CE-miR134-RNAi, miR134-RNAi-injected CE mice.

but not astrocytes or microglia, in naive mice. In addition, we injected an adeno-associated virus (AAV9-mmu-miR134-5P-RNAi-GFP) to knock down the expression of miR134 in the vHP, which also primarily transacted into the neurons (NeuN as a marker) but not the GFAP- and Iba-1-positive glial cells. These results indicated that miR134 mainly localized in the glutamatergic neurons in the vHP. Studies have shown that miR134 negatively regulates the develop-

ment of dendritic spine and synaptic plasticity in the hippocampus.^{15,37} In the present study, some target genes of miR134, such as *Sypl2*, *Snap23*, *Bdnf*, and *Creb1*, have been reported to play important roles in dendritic spine and synaptic plasticity,^{38–40} raising the possibility that vHP miR134 might modulate behaviors via regulating the synaptic plasticity. The number of dendritic spines is closely associated with the strength of excitatory transmission.^{41,42} An *in vivo* study

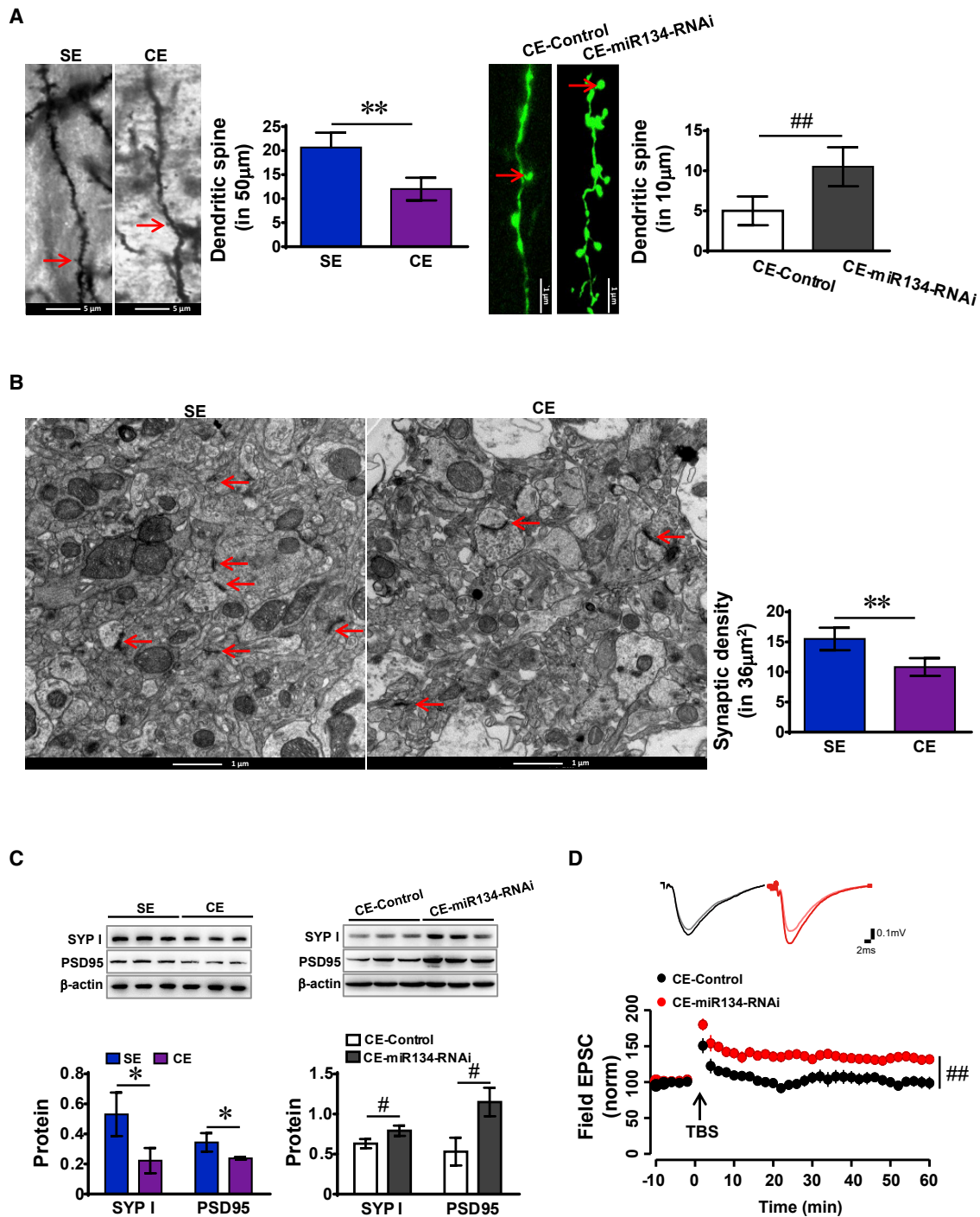


Figure 5. Knockdown of miR134 in the vHP Ameliorates CE-Induced Changes in Synaptic Plasticity of the vHP

(A) Dendritic spines. Representative images of dendritic spines in the vHP of SE and CE mice (left, $n = 12$; scale bars, 5 μ m), as well as in miR134 RNAi and controlled RNAi of CE mice (right, $n = 12$; scale bars, 1 μ m). Red arrows indicate the spines. (B) Synapses. Representative images of synapses (left) and graph of synaptic density (right, $n = 12$) in the vHP of SE and CE mice. Red arrows indicate synapses. Scale bars, 1 μ m. (C) Protein levels of synapsin I (SYP I) and PSD-95 in the vHP of SE and CE mice (left, $n = 6$), as well as in miR134 RNAi and controlled RNAi of CE mice (right, $n = 6$). (D) fEPSP of the vHP in miR134 RNAi and controlled RNAi of CE mice. Representative traces of EPSP (top) and slopes of EPSP (bottom; $n = 12$) of vHP in controlled RNAi and miR134 RNAi mice. * $p < 0.05$ and ** $p < 0.01$, versus SE mice; # $p < 0.05$ and ## $p < 0.01$, versus CE-control mice. CE, cocaine extinction mice; SE, saline extinction mice; CE-control, controlled RNAi-injected CE mice; CE-miR134-RNAi, miR134-RNAi-injected CE mice.

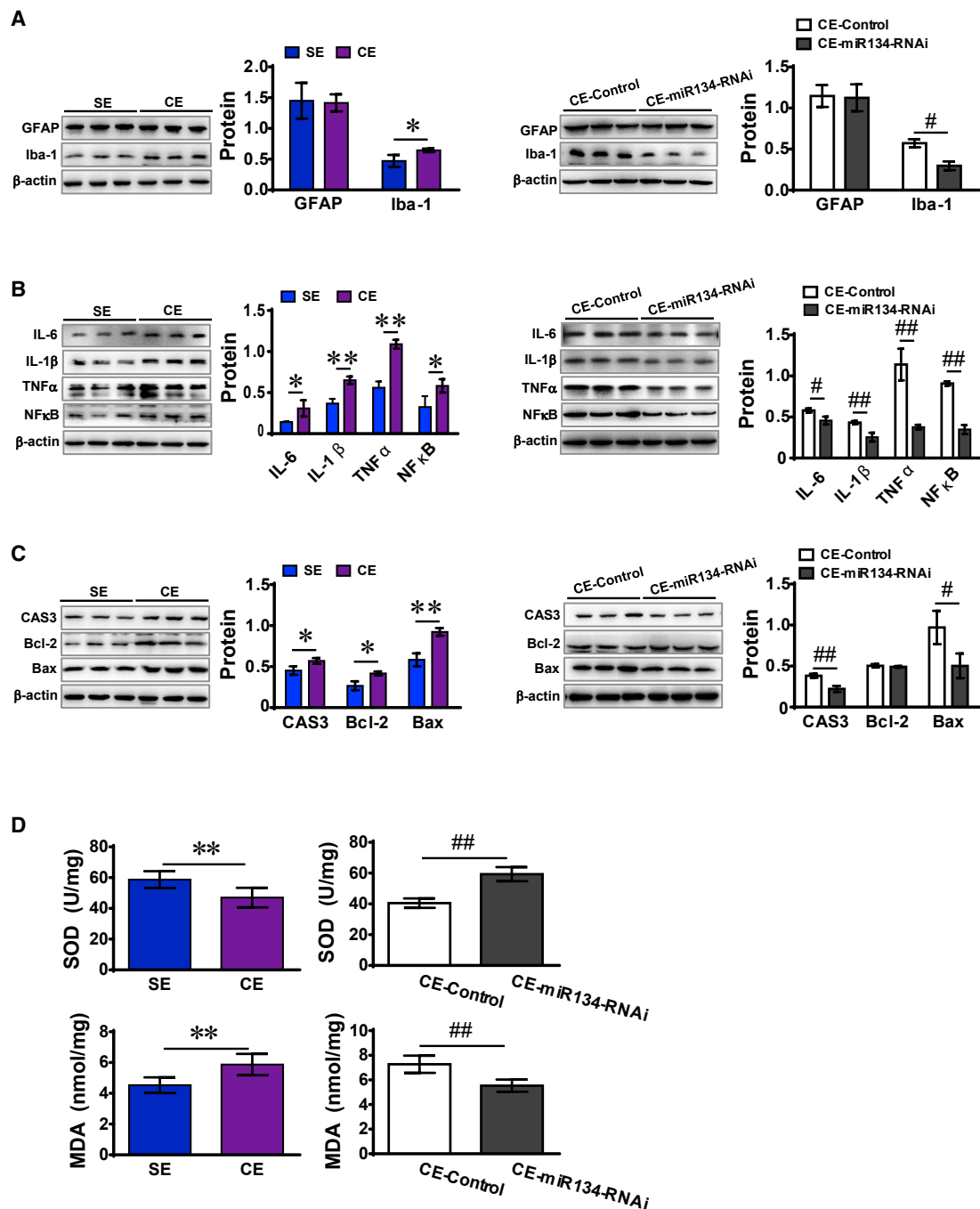


Figure 6. Knockdown of miR134 in the vHP Relieves the Enhancements in Microglia Activity and Inflammatory, Apoptotic, and Oxidative Stress Statuses of CE Mice

(A) Protein levels of GFAP and Iba-1 in the vHP of SE and CE mice (left, n = 6), as well as in miR134 RNAi and controlled RNAi of CE mice (right, n = 6). (B) Protein levels of pro-inflammatory factors in the vHP of SE and CE mice (left, n = 6), as well as in miR134 RNAi and controlled RNAi of CE mice (right, n = 6). (C) Protein levels of apoptotic molecules in the vHP of SE and CE mice (left, n = 6), as well as in miR134 RNAi and controlled RNAi of CE mice (right, n = 6). (D) Activities of SOD (top) and level of MDA (bottom) in the vHP of SE and CE mice (left, n = 12), as well as in miR134 RNAi and controlled RNAi of CE mice (right, n = 12). *p < 0.05 and **p < 0.01, versus SE mice; #p < 0.05 and ##p < 0.01, versus CE-control mice. CE, cocaine extinction mice; SE, saline extinction mice; CE-control, controlled RNAi-injected CE mice; CE-miR134-RNAi, miR134-RNAi-injected CE mice.

showed that higher levels of miR134 negatively regulate EPSP in the hippocampus via blockade of key plasticity proteins such as CREB.¹⁵ Consistent with this finding, we found that both densities of dendritic spines and synapses, as well as the levels of synaptic proteins, including SYP I and PSD-95, were significantly reduced by CE in the vHP of mice, suggesting an attenuated synaptic transmission in the vHP by CE. Most importantly, local knockdown of vHP miR134 *in vivo* restored the decreased levels of synaptic proteins, accompanied by an enhanced fEPSC in the CA1 of vHP, indicating that miR134 negatively regulates excitatory transmission in mice during the CE period.

Most studies demonstrate the negative regulation of miR134 on hippocampal dendritic spine size⁹ and density.¹⁵ However, one recent study found that silencing miR134 in the pyramidal neurons of hippocampus could reduce spine density in prolonged-seizure animals, which could suppress seizures.⁷ Dendritic spines are targets of excitatory axons in the brain;^{41,43} thus, spine loss is supposed to result in the attenuation of excitatory responses.⁴⁴ The reason for the discrepancy among studies may be due to the different disease models and different sub-region of hippocampus studied.

miR134 Is Involved in CE-Caused Changes in Neurochemical Environments in vHP of Mice

In recent decades, increasing evidence has demonstrated that the microenvironment of the neuron could be damaged by these addictive drugs, always being due to the overactive glial cells, oxidative stress, or inflammatory or apoptotic status around neurons.^{45–49} Thus, rescuing the microenvironment in the brain might be a common and effective therapeutic approach for treatment of addiction and related psychiatric disorders.

miR134 has been reported to be involved in inflammation, oxidative stress, mitochondrial function, apoptosis, and autophagy in the hippocampus.^{25,50–52} Here, knockdown of vHP miR134 suppressed CE-enhanced oxidative molecules, pro-inflammatory and pro-apoptotic factors in the vHP. Microglia, but not astrocytes, were reversed by miR134 inhibition, indicating that microglia may be potential intervention targets for miR134. Since we found that miR134 was mainly expressed in neurons of vHP but not glial cells, there must be a crosstalk mechanism between neurons and glia that miR134 plays its regulatory roles in the glia activities and neurochemical microenvironments.

In summary, our studies link miR134 with the increased anxiety and depression by CE exposure. A limitation of this study is not identifying the role of miR134 in the crosstalk between neuron and glial cells under the condition of cocaine abuse. The results of this study demonstrate that the miR134 signaling pathway in the vHP contributes to the development of drug-related psychiatric problems, mechanically through regulating synaptic plasticity and microenvironment. miR134 may be a promising therapeutic target for the treatment of drug-related psychiatric disorders and a potential biomarker to evaluate the therapeutic efficacy against addiction.

MATERIALS AND METHODS

All experiments were performed in accordance with the Nanjing University of Chinese Medicine Guide for the Care and Use of Laboratory Animals, Nanjing, China. The study has been approved by the Nanjing University of Chinese Medicine Institutional Animal Care and Use Committee.

Animals

C57BL/6 male mice were maintained on a reverse light:dark cycle with food and water available *ad libitum*. All mice were allowed to acclimate for 7 days before receiving any experimental manipulation. Mice were assigned to receive a daily injection of cocaine hydrochloride (15 mg/kg in saline, intraperitoneally [i.p.], Qinghai Pharmaceutical, Qinghai, China) or saline for 14 consecutive days. CPP procedures were performed in all mice. Some cocaine-experienced mice were subjected to local knockdown treatment of miR134 in the vHP. Brain tissue was collected on day 33 from some mice, and the behavioral tests were carried out from day 34 in the other mice (Figure 1B).

Behavior Tests

CPP

Cocaine CPP procedures were performed as described previously.¹⁰ The TopScan3D CPP apparatus (CleverSys, Reston, VA, USA) is constructed of two distinct chambers separated by a removable guillotine door. The CPP procedure consisted of five phases: the pre-conditioning test (pre-test, day –1), acquisition conditioning (days 0–14), post-conditioning test (CPP test, day 15), extinction training (days 16–31), and extinction test (day 32). During CPP acquisition conditioning, mice received an injection of saline (0.2 mL per mouse) or cocaine (15 mg/kg, i.p.) once daily and were kept in one fixed chamber (drug-paired chamber) for 45 min. To train CPP extinction, mice were confined to the drug-paired chamber for 45 min once daily without any drug treatment. During the pre-test, CPP test, and extinction test, mice were allowed to freely access two chambers for 15 min. Time spent in the drug-paired chamber was recorded as the CPP score. Mice that exhibited cocaine-extinct CPP were defined as CE mice, and saline-extinct CPP mice served as SE mice.

Anxiety-like and Depression-like Behavior Tests

Anxiety levels were evaluated with the EPM on day 34 and the OFT on day 37. Time in the open arms and central zone (measured using the EPM and OFT, respectively) were calculated. Depression levels were evaluated with the TST on day 40 and the FST on day 43. The movement status of each mouse was recorded for 6 min. Immobility time during the last 4 min of the tests was measured.

The EPM apparatus consists of four elevated arms (70 cm above the floor) arranged in a cross pattern with two 1-cm walled arms (open arms) and two 40-cm walled arms (close arms). Mice were released from the central platform individually, and the behaviors were recorded for 5 min with a camera positioned overhead. Between each trial, the maze was cleaned with ethanol and water. The time spent in the open arms was measured.

In the OFT, mice were placed gently in the center of the open field apparatus (60 cm × 60 cm) individually, and the behaviors were recorded for 5 min with a camera positioned overhead. The time spent in the central zone (30 cm × 30 cm) and the distance traveled in the apparatus were measured.

In the TST, each mouse was suspended 40 cm above the tabletop surface with adhesive tape placed 1 cm from the tip of the tail. Movement was recorded using a camera for 6 min, and the immobility duration in the last 4 min was calculated. Mice were considered immobile only when they hung motionless.

In the FST, mice were placed individually in a clear plastic cylinder (45 cm high, 20-cm diameter) filled with 30 cm of water (25°C). Immobile time during last 4 min of the 6-min test was scored. Mice were judged to be in an immobile state whenever they remained floating in the water without struggling and only made movements necessary to remain afloat. Latency to immobility was defined as the time between an introduction to the chamber and the first instance of immobility.

Virus Injection

Mice were anesthetized with isoflurane and injected with 0.5 μ L AAV9-mmu-miR134-5P-RNAi-GFP virus or control virus into the bilateral vHP (Figure 2B). The vHP coordinates were as follows: anterior-posterior (AP), -3.4 mm; medial-lateral (ML), ± 2.8 mm; and dorsal-ventral (DV), -5.0 mm.⁵³ Infusions were made with a syringe pump at a rate of 0.2 μ L/min connected to Hamilton syringes attached via polyethylene tubing to injectors. The injectors were kept in place for an additional 5 min to allow for virus diffusion. The detailed information about AAV9-mmu-miR134-5P-RNAi-GFP is presented in Supplemental Methods.

Immunofluorescence

Mice were perfused with 4% paraformaldehyde (PFA) in PBS buffer (pH 7.4). The brains were removed and post-fixed in the same 4% PFA for 2 h and then were put in 30% sucrose overnight and cut on cryostat to form frozen coronal sections (15 μ m). Frozen sections were incubated at 4°C overnight with primary antibodies, CaMKII (1:1,000 dilution, Cell Signaling Technology, Danvers, MA, USA), GFAP (1:500 dilution, Abcam, Cambridge, MA, USA), Iba-1 (1:500 dilution, Wako Pure Chemicals Industries, Osaka, Japan), and NeuN (1:500 dilution, Abcam, Cambridge, MA, USA). Then, the sections were incubated with the Cy3- and fluorescein isothiocyanate (FITC)-labeled secondary antibodies (1:100 dilution, Sigma, St. Louis, MO, USA) at 37°C for 1 h. Negative control sections were performed by replacing the primary antibodies with PBS buffer. The number of double-stained cells was counted by software (Leica, Wetzlar, Germany).

BaseScope Assay

Single-molecule miRNA fluorescent *in situ* hybridization was performed using BaseScope probes (ACDBio, Newark, CA, USA) according to the manufacturer's protocol. Mouse brains were perfused

with freshly prepared 4% PFA in 1 × PBS, and then, brains were dissected and placed in 4% PFA for 24 h at 4°C. Brains were immersed in 30% sucrose in 1 × PBS at 4°C until they sank to the bottom of the container. Fresh frozen mouse brains were sectioned at 15- μ m thickness on a cryostat (Leica, Wetzlar, Germany). Slides were baked in a dry-air oven for 30 min at 60°C, and then slides were washed with 1 × PBS for 5 min. RNAscope Hydrogen Peroxide was added for 10 min at room temperature (RT). Next, the slide rack was submerged into the hot 1 × RNAscope Target Retrieval solution for 5 min and immediately transferred to distilled water. Slides were washed in fresh 100% EtOH and air dried. The slides were incubated with RNAscope Pro tease Plus at 40°C for 30 min. Mouse miRNA134 probe (#726821) was used for detecting miR134, and DapB-1ZZ probe (#701021) was used as a negative control. Then, we proceeded to the normal immunofluorescence assay described previously after performing the RNAscope 2.5 HD RED assay. Images were obtained from consecutive sections, using the same exact camera settings under a Leica DM6B upright digital research microscope at 20× original magnification.

Reverse Transcription and Quantitative Real-time PCR

RNA isolation, reverse transcription and quantitative real-time PCR (qPCR) procedures were performed as described previously.¹⁰ In brief, total RNA were reversely transcribed and analysis of qPCR reaction was performed using the SYBR Green PCR Master Mix Kit (SuperArray Bioscience, Frederick, MD, USA) and the ABI 7900HT Fast Real-Time PCR System (Applied Biosystems, Beverly, MA, USA). miR134-5P and 49 potential gene targets were quantified in the vHP. The specific primer for mmu-miR134-5P was as follows: 5'-TGTGACTGGTTGACCAGAGG-3'. Other primers of this study are listed in Supplemental Methods. The expression of U6 small nucleolar RNA and Gapdh was used as the internal control for miR134-5P and gene targets, respectively. The relative expression level was calculated by the comparative CT method ($2^{-\Delta\Delta Ct}$).

Dendritic Spine Counting

Mice were deeply anesthetized with isoflurane and decapitated, and the vHP region was separated immediately. In this study, dendrites and spines were stained using the Golgi staining method and the GFP-labeled virus method.

The Golgi staining procedure was carried out according to the manufacturer's instructions for the FD Rapid GolgiStain Kit (FD NeuroTechnologies, Columbia, MD, USA). Sections were cut at 100 μ m on a cryostat. Individual pyramidal neurons were selected from CA1 and traced on a microscope (Leica Microsystems, Wetzlar, Germany). The spines on secondary and tertiary dendrites of neurons were calculated at a dendritic segment length of 50 μ m.

The virus used in this study is GFP-labeled AAV9, which can be transduced and expressed in the pyramidal neurons of vHP CA1. Dendritic spines can be shown by GFP expression. The spines on the secondary and tertiary dendrites of neurons were calculated at a dendritic segment length of 10 μ m.

Synaptic Density

Transmission electron microscopy (TEM) was used to observe the structure of the vHP. Mouse brains were removed, and the vHP region was separated immediately on ice. The vHP was fixed in glutaraldehyde at 4°C for 6 h. Sections were post-fixed by immersion in 1% OsO₄ for 2 h at room temperature and dehydrated in graded alcohol solution and embedded in propylene oxide. 60-nm sections were stained with uranyl acetate and lead citrate and imaged using the Tecnai G2 Spirit Bio TWIN (FEI, Eindhoven, the Netherlands).

Western Blot

Western blot was performed as described previously.⁵ Total protein was extracted using RIPA lysis buffer (Beyotime Institute of Biotechnology, Beijing, China). Protein samples (30 µg) were loaded and electrophoresed on 10% SDS-PAGE gels and transferred to polyvinylidene fluoride (PVDF) membranes. Membranes were incubated with one of the following primary antibodies at 4°C overnight: SYP I (Signalway Antibody, College Park, MD, USA); PSD-95 (Signalway Antibody, College Park, MD, USA); β-actin (Santa Cruz Biotechnology, Santa Cruz, CA, USA); GFAP (Abcam, Cambridge, MA, USA); Iba-1 (Boster Biotechnology, Wuhan, China); IL-6 (Boster Biotechnology, Wuhan, China); IL-1β (Boster Biotechnology, Wuhan, China); TNF-α (Boster Biotechnology, Wuhan, China); NF-κB (Boster Biotechnology, Wuhan, China); CAS3 (Boster Biotechnology, Wuhan, China); Bcl-2 (Boster Biotechnology, Wuhan, China); and Bax (Boster Biotechnology, Wuhan, China). The membranes were washed with Tris-Buffered Saline with Tween-20 (TBST) and then incubated with horseradish peroxidase (HRP)-conjugated secondary antibody (Santa Cruz Biotechnology, Dallas, TX, USA) for 1 h at room temperature. The blots were visualized by an enhanced chemiluminescence (ECL) kit (Beyotime Institute of Biotechnology, Beijing, China). Quantitative analysis of density was normalized to β-actin protein expression.

Oxidative Stress Assays

The protocols were performed as described previously.⁵ The samples were homogenized and centrifuged, and then the supernatant was used for the oxidative stress assay. Commercial detection kits (Jiancheng Bioengineering Institute, Nanjing, China) were used to measure the activity of SOD and the level of MDA according to the manufacturer's instructions.

fEPSP Recording

For brain slice preparation, mice were deeply anesthetized with isoflurane and decapitated. Brains were quickly removed and submerged in cutting solution (in millimolar as follows: 119 NaCl, 2.5 KCl, 6 kynurenic acid, 1 NaH₂PO₄, 13.5 glucose, 100.1 sucrose, 77.9 NaHCO₃, 3.5 CaCl₂, and 7.3 MgCl₂). Horizontal sections (350 µm) containing the vHP were cut using a vibratome (Leica Microsystems, Wetzlar, Germany) in ice-cold cutting solution. Brain slices were submerged in ACSF (artificial cerebrospinal fluid in millimolar as follows: 119 NaCl, 2.5 KCl, 1 NaH₂PO₄, 11 glucose, 26.2 NaHCO₃, 2.5 CaCl₂, and 1.3 MgCl₂) at 32°C for 30 min and equilibrated with 95% O₂

and 5% CO₂. Slices were then individually transferred to the recording chamber and superfused continuously with 28°C ACSF.

For extracellular recording, the electrodes were filled with ACSF and placed in the stratum radiatum of the CA1. Resistance varied from 3 to 4 MΩ. A bipolar stimulating electrode used to evoke fEPSP was placed on the pathway from CA3 to CA1. Adjusted stimulus, which evoked 40%–50% of the maximum response, was delivered at 0.066 Hz. After 30 min of stable baseline recording, LTP was induced via four theta burst stimulation (TBS) trains (each with 10 bursts containing 4 pulses at 100 Hz and repeating at 5 Hz), given at 20-s intervals. Slopes of eight consecutive fEPSP responses were averaged as an index for synaptic intensity.

Statistical Analyses

Statistical analysis was carried out using GraphPad Prism software. All results are expressed as mean ± SD, and data between groups were compared using two-tailed Student's t test. *p* < 0.05 was considered significant in all tests.

SUPPLEMENTAL INFORMATION

Supplemental Information can be found online at <https://doi.org/10.1016/j.omtn.2019.12.030>.

AUTHOR CONTRIBUTIONS

X.G. conceptualized the research and designed the experiments. Y.L., X.L., and J.N. performed the behavioral and biochemical experiments. Y.L., X.L., and P.H. performed morphological experiments. F.G. and T.-F.Y. performed electrophysiological experiments. X.G., F.G., and T.-F.Y. analyzed the data and wrote the manuscript. All authors read and approved the final manuscript.

CONFLICTS OF INTEREST

The authors declare no competing interests.

ACKNOWLEDGMENTS

This work was supported by the National Natural Science Foundation of China (81571303 and 81371467); the Open Project Program of Jiangsu Key Laboratory for Pharmacology and Safety Evaluation of Chinese Materia Medica (JKPLSE201814); the Project of the Priority Academic Program Development of Jiangsu Higher Education Institutions (PAPD); and the Priority Academic Program Development of Jiangsu Higher Education Institutions (Integration of Chinese and Western Medicine) to X.G. The authors report no biomedical financial interests.

REFERENCES

1. Jonkman, S., and Kenny, P.J. (2013). Molecular, cellular, and structural mechanisms of cocaine addiction: a key role for microRNAs. *Neuropsychopharmacology* 38, 198–211.
2. Buffalari, D.M., Baldwin, C.K., and See, R.E. (2012). Treatment of cocaine withdrawal anxiety with guanfacine: relationships to cocaine intake and reinstatement of cocaine seeking in rats. *Psychopharmacology (Berl.)* 223, 179–190.

3. Elman, I., Karlsgodt, K.H., Gastfriend, D.R., Chabris, C.F., and Breiter, H.C. (2002). Cocaine-primed craving and its relationship to depressive symptomatology in individuals with cocaine dependence. *J. Psychopharmacol. (Oxford)* 16, 163–167.
4. Rincón-Cortés, M., Gagnon, K.G., Dollish, H.K., and Grace, A.A. (2018). Diazepam reverses increased anxiety-like behavior, social behavior deficit, and dopamine dysregulation following withdrawal from acute amphetamine. *Neuropsychopharmacology* 43, 2418–2425.
5. Hu, P., Zhu, W., Zhu, C., Jin, L., Guan, Y., and Guan, X. (2016). Resveratrol fails to affect cocaine conditioned place preference behavior, but alleviates anxiety-like behaviors in cocaine withdrawn rats. *Psychopharmacology (Berl.)* 233, 1279–1287.
6. Kampman, K.M., Dackis, C., Lynch, K.G., Pettinati, H., Tirado, C., Gariti, P., Sparkman, T., Atzram, M., and O'Brien, C.P. (2006). A double-blind, placebo-controlled trial of amantadine, propranolol, and their combination for the treatment of cocaine dependence in patients with severe cocaine withdrawal symptoms. *Drug Alcohol Depend.* 85, 129–137.
7. Jimenez-Mateos, E.M., Engel, T., Merino-Serrais, P., McKiernan, R.C., Tanaka, K., Mouri, G., Sano, T., O'Tuathaigh, C., Waddington, J.L., Prenter, S., et al. (2012). Silencing microRNA-134 produces neuroprotective and prolonged seizure-suppressive effects. *Nat. Med.* 18, 1087–1094.
8. Saugstad, J.A. (2010). MicroRNAs as effectors of brain function with roles in ischemia and injury, neuroprotection, and neurodegeneration. *J. Cereb. Blood Flow Metab.* 30, 1564–1576.
9. Schrott, G.M., Tuebing, F., Nigh, E.A., Kane, C.G., Sabatini, M.E., Kiebler, M., and Greenberg, M.E. (2006). A brain-specific microRNA regulates dendritic spine development. *Nature* 439, 283–289.
10. Chen, C.L., Liu, H., and Guan, X. (2013). Changes in microRNA expression profile in hippocampus during the acquisition and extinction of cocaine-induced conditioned place preference in rats. *J. Biomed. Sci.* 20, 96.
11. Pilakka-Kanthikeel, S., and Nair, M.P. (2015). Interaction of drugs of abuse and microRNA with HIV: a brief review. *Front. Microbiol.* 6, 967.
12. Martinetz, S. (2016). MicroRNA's impact on neurotransmitter and neuropeptide systems: small but mighty mediators of anxiety. *Pflugers Arch.* 468, 1061–1069.
13. O'Connor, R.M., Dinan, T.G., and Cryan, J.F. (2012). Little things on which happiness depends: microRNAs as novel therapeutic targets for the treatment of anxiety and depression. *Mol. Psychiatry* 17, 359–376.
14. Doura, M.B., and Unterwald, E.M. (2016). MicroRNAs modulate interactions between stress and risk for cocaine addiction. *Front. Cell. Neurosci.* 10, 125.
15. Gao, J., Wang, W.Y., Mao, Y.W., Gráff, J., Guan, J.S., Pan, L., Mak, G., Kim, D., Su, S.C., and Tsai, L.H. (2010). A novel pathway regulates memory and plasticity via SIRT1 and miR-134. *Nature* 466, 1105–1109.
16. Jimenez-Mateos, E.M., Engel, T., Merino-Serrais, P., Feraud-Espinosa, I., Rodriguez-Alvarez, N., Reynolds, J., Reschke, C.R., Conroy, R.M., McKiernan, R.C., deFelipe, J., and Henshall, D.C. (2015). Antagomirs targeting microRNA-134 increase hippocampal pyramidal neuron spine volume in vivo and protect against pilocarpine-induced status epilepticus. *Brain Struct. Funct.* 220, 2387–2399.
17. Wang, X.M., Jia, R.H., Wei, D., Cui, W.Y., and Jiang, W. (2014). MiR-134 blockade prevents status epilepticus like-activity and is neuroprotective in cultured hippocampal neurons. *Neurosci. Lett.* 572, 20–25.
18. Meng, F., Li, Y., Chi, W., and Li, J. (2016). Morphine preconditioning downregulates microRNA-134 expression against oxygen-glucose deprivation injuries in cultured neurons of mice. *J. Neurosurg. Anesthesiol.* 28, 195–202.
19. Rogers, J.L., and See, R.E. (2007). Selective inactivation of the ventral hippocampus attenuates cue-induced and cocaine-primed reinstatement of drug-seeking in rats. *Neurobiol. Learn. Mem.* 87, 688–692.
20. Lasseter, H.C., Xie, X., Ramirez, D.R., and Fuchs, R.A. (2010). Sub-region specific contribution of the ventral hippocampus to drug context-induced reinstatement of cocaine-seeking behavior in rats. *Neuroscience* 171, 830–839.
21. Trivedi, M.A., and Coover, G.D. (2004). Lesions of the ventral hippocampus, but not the dorsal hippocampus, impair conditioned fear expression and inhibitory avoidance on the elevated T-maze. *Neurobiol. Learn. Mem.* 81, 172–184.
22. Albrecht, A., Çalıřkan, G., Oitzl, M.S., Heinemann, U., and Stork, O. (2013). Long-lasting increase of corticosterone after fear memory reactivation: anxiolytic effects and network activity modulation in the ventral hippocampus. *Neuropsychopharmacology* 38, 386–394.
23. Chi, W., Meng, F., Li, Y., Li, P., Wang, G., Cheng, H., Han, S., and Li, J. (2014). Impact of microRNA-134 on neural cell survival against ischemic injury in primary cultured neuronal cells and mouse brain with ischemic stroke by targeting HSPA12B. *Brain Res.* 1592, 22–33.
24. Fan, C., Zhu, X., Song, Q., Wang, P., Liu, Z., and Yu, S.Y. (2018). MiR-134 modulates chronic stress-induced structural plasticity and depression-like behaviors via down-regulation of Limk1/cofilin signaling in rats. *Neuropharmacology* 131, 364–376.
25. Sun, J., Gao, X., Meng, D., Xu, Y., Wang, X., Gu, X., Guo, M., Shao, X., Yan, H., Jiang, C., and Zheng, Y. (2017). Antagomirs targeting miRNA-134 attenuates epilepsy in rats through regulation of oxidative stress, mitochondrial functions and autophagy. *Front. Pharmacol.* 8, 524.
26. Ji, L.J., Su, J., Xu, A.L., Pang, B., and Huang, Q.M. (2018). MiR-134-5p attenuates neuropathic pain progression through targeting Twist1. *J. Cell Biochem.* Published September 6, 2018. <https://doi.org/10.1002/jcb.27486>.
27. Yamakuchi, M. (2012). MicroRNA regulation of SIRT1. *Front. Physiol.* 3, 68.
28. McClung, C.A., and Nestler, E.J. (2008). Neuroplasticity mediated by altered gene expression. *Neuropsychopharmacology* 33, 3–17.
29. Ambros, V. (2004). The functions of animal microRNAs. *Nature* 431, 350–355.
30. Zhang, J., Ma, Y., Wang, S., Chen, F., and Gu, Y. (2015). C/EBP α inhibits proliferation of breast cancer cells via a novel pathway of miR-134/CREB. *Int. J. Clin. Exp. Pathol.* 8, 14472–14478.
31. Baby, N., Alagappan, N., Dheen, S.T., and Sajikumar, S. (2019). MicroRNA-134-5p inhibition rescues long-term plasticity and synaptic tagging/capture in an A β (1-42)-induced model of Alzheimer's disease. *Aging Cell*, e13046. Published online October 17, 2019. <https://doi.org/10.1111/acel.13046>.
32. Antolin-Fontes, B., Ables, J.L., Görlich, A., and Ibañez-Tallon, I. (2015). The habenulo-interpeduncular pathway in nicotine aversion and withdrawal. *Neuropharmacology* 96 (Pt B), 213–222.
33. Shen, J., Xu, L., Qu, C., Sun, H., and Zhang, J. (2018). Resveratrol prevents cognitive deficits induced by chronic unpredictable mild stress: Sirt1/miR-134 signalling pathway regulates CREB/BDNF expression in hippocampus in vivo and in vitro. *Behav. Brain Res.* 349, 1–7.
34. McCarthy, D.M., Brown, A.N., and Bhide, P.G. (2012). Regulation of BDNF expression by cocaine. *Yale J. Biol. Med.* 85, 437–446.
35. Larson, E.B., Graham, D.L., Arzaga, R.R., Buzin, N., Webb, J., Green, T.A., Bass, C.E., Neve, R.L., Terwilliger, E.F., Nestler, E.J., and Self, D.W. (2011). Overexpression of CREB in the nucleus accumbens shell increases cocaine reinforcement in self-administering rats. *J. Neurosci.* 31, 16447–16457.
36. Numakawa, T., Nakajima, S., Yamamoto, N., Ooshima, Y., Odaka, H., Hashido, K., Adachi, N., and Kunugi, H. (2015). Basic fibroblast growth factor induces miR-134 upregulation in astrocyte for cell maturation. *Biochem. Biophys. Res. Commun.* 456, 465–470.
37. Christensen, M., Larsen, L.A., Kauppinen, S., and Schrott, G. (2010). Recombinant adeno-associated virus-mediated microRNA delivery into the postnatal mouse brain reveals a role for miR-134 in dendritogenesis in vivo. *Front. Neural Circuits* 3, 16.
38. Frank, D.A., and Greenberg, M.E. (1994). CREB: a mediator of long-term memory from mollusks to mammals. *Cell* 79, 5–8.
39. Flavell, S.W., and Greenberg, M.E. (2008). Signaling mechanisms linking neuronal activity to gene expression and plasticity of the nervous system. *Annu. Rev. Neurosci.* 31, 563–590.
40. Skalska, J., Frontczak-Baniewicz, M., and Strużyńska, L. (2015). Synaptic degeneration in rat brain after prolonged oral exposure to silver nanoparticles. *Neurotoxicology* 46, 145–154.
41. Matsuzaki, M., Honkura, N., Ellis-Davies, G.C., and Kasai, H. (2004). Structural basis of long-term potentiation in single dendritic spines. *Nature* 429, 761–766.
42. Zito, K., Knott, G., Shepherd, G.M., Shenolikar, S., and Svoboda, K. (2004). Induction of spine growth and synapse formation by regulation of the spine actin cytoskeleton. *Neuron* 44, 321–334.

43. Zhou, Q., Homma, K.J., and Poo, M.M. (2004). Shrinkage of dendritic spines associated with long-term depression of hippocampal synapses. *Neuron* 44, 749–757.
44. Müller, M., Gähwiler, B.H., Rietschin, L., and Thompson, S.M. (1993). Reversible loss of dendritic spines and altered excitability after chronic epilepsy in hippocampal slice cultures. *Proc. Natl. Acad. Sci. USA* 90, 257–261.
45. Cooper, Z.D., Jones, J.D., and Comer, S.D. (2012). Glial modulators: a novel pharmacological approach to altering the behavioral effects of abused substances. *Expert Opin. Investig. Drugs* 21, 169–178.
46. Liu, L.W., Lu, J., Wang, X.H., Fu, S.K., Li, Q., and Lin, F.Q. (2013). Neuronal apoptosis in morphine addiction and its molecular mechanism. *Int. J. Clin. Exp. Med.* 6, 540–545.
47. López-Pedrajas, R., Ramírez-Lamelas, D.T., Muriach, B., Sánchez-Villarejo, M.V., Almansa, I., Vidal-Gil, L., Romero, F.J., Barcia, J.M., and Muriach, M. (2015). Cocaine promotes oxidative stress and microglial-macrophage activation in rat cerebellum. *Front. Cell. Neurosci.* 9, 279.
48. Ray, L.A., Roche, D.J., Heinzerling, K., and Shoptaw, S. (2014). Opportunities for the development of neuroimmune therapies in addiction. *Int. Rev. Neurobiol.* 118, 381–401.
49. Scofield, M.D., and Kalivas, P.W. (2014). Astrocytic dysfunction and addiction: consequences of impaired glutamate homeostasis. *Neuroscientist* 20, 610–622.
50. Ni, J., Gao, Y., Gong, S., Guo, S., Hisamitsu, T., and Jiang, X. (2013). Regulation of μ -opioid type 1 receptors by microRNA134 in dorsal root ganglion neurons following peripheral inflammation. *Eur. J. Pain* 17, 313–323.
51. Liao, T.L., Chen, Y.M., Hsieh, C.W., Chen, H.H., Lee, H.C., Hung, W.T., Tang, K.T., and Chen, D.Y. (2017). Upregulation of circulating microRNA-134 in adult-onset Still's disease and its use as potential biomarker. *Sci. Rep.* 7, 4214.
52. Huang, W., Meng, F., Cao, J., Liu, X., Zhang, J., and Li, M. (2017). Neuroprotective role of exogenous brain-derived neurotrophic factor in hypoxia-hypoglycemia-induced hippocampal neuron injury via regulating Trkb/MiR134 signaling. *J. Mol. Neurosci.* 62, 35–42.
53. Franklin, K.B.J., and Paxinos, G. (1997). *The Mouse Brain in Stereotaxic Coordinates* (Academic Press).